Ag nanoparticle-decorated SiO2@TiO2 hierarchical microspheres improve the efficiency of dye-sensitized solar cells

Junchen Sun
Anhui University
Min Fang
Anhui University
Weiju Zhu
Anhui University
Zhenyu Wu
Anhui University
Cun Li (cun_li@126.com)
Anhui University School of Chemistry and Chemical Engineering https://orcid.org/0000-0001-9076-4802

Research Article

Keywords: SiO2@TiO2-Ag microspheres, Light scatter, Localized surface plasmon resonance (LSPR), Dye-sensitized solar cells (DSSCs)

Posted Date: June 21st, 2021

DOI: https://doi.org/10.21203/rs.3.rs-363255/v1

Version of Record: A version of this preprint was published at Journal of Materials Science: Materials in Electronics on July 17th, 2021. See the published version at https://doi.org/10.1007/s10854-021-06466-5.

Abstract

SiO_2@TiO_2-Ag (STA) microspheres decorated with Ag nanoparticles (Ag NPs) were prepared and assembled into the photoanode. The photoanode composed of STA microspheres and TiO_2 nanoparticles (P25) was prepared by doctor blade method. UV-vis measurement indicates that the introduction of a few STA microspheres observably enhance the light scattering and capturing ability of the photoanode. The photoelectric conversion efficiency of the DSSCs with 2wt% STA photoanode increased to 7.4% from 4.3% comparing with pure P25 TiO_2 nanoparticles. The configuration DSSCs have the maximum short circuit current density (J_{sc}) of 16.0 mA cm^{-2} and open circuit voltage (V_{oc}) of 0.780 V, which are significantly higher than the pure TiO_2 DSSCs. The significant improvement of the DSSCs performance can be due to the synergistic effect of the superior light scattering of STA and the localized surface plasma resonance (LSPR) effect of Ag NPs modified on the microspheres surface.

1 Introduction

Dye-sensitized solar cells (DSSCs) have attracted huge attention in recent years due to their relatively low cost, easy production process and moderate photovoltaic performance since designed by Gratzel team in 1991 [1]. Generally, a typical DSSCs is composed of a photoanode, a counter electrode (CE), the electrolyte and the photo-sensitizer (dye) [2]. The photoanode plays an important role to achieve high photoelectric conversion efficiency (PCE), which usually is made of porous metal oxide semiconductors such as TiO_2, ZnO, SnO_2, etc [3]. Among them,TiO_2 has aroused extensive attention due to its suitable band-edge position, anti-photocorrosion stability, and nontoxicity [4]. However, the intrinsic low carrier mobility and the weaker light capture rate of TiO_2 severely limits the efficiency of DSSCs [5]. The low carrier mobility makes electron hole recombination easier. The nanocrystals in small size have higher transparency, resulting in lower light capture rate. To solve the above problems, design of photoanode materials with strong light capture and efficient electron transfer capacity has become a research hotspot. Nowadays, various methods are used to optimize the photoanode to improve the photovoltaic property of DSSCs by acid surface modification, metallic oxide doping and introduction of scattering layer [6–8].

Adding light scattering material into the photoanode is a simple and feasible method to increase the light absorption and increase the performance of the DSSCs. The incident light can be reflected and scattered when passing through the photoanode film, so that improves the absorption and capture ability of light. In general, the scattering material is introduced into the photoanode with double-layer or hybrid structure. Yu Group has fabricated layered TiO_2 microspheres as the scattering layer in DSSCs, and the performance of the cell has been significantly improved [9]. Son group has reported that SiO_2/TiO_2 spheres consisting of a low refractive index core and high refractive index shell enhanced light scattering to improve power conversion efficiency of DSSCs [10]. Tan and Wu group prepared composite solar cells by using anatase nanoparticles and single crystal anatase TiO_2 nanowires. The DSSCs based on TiO_2 nanowire have light scattering effect and electron fast transmission channel, which make the efficiency

of the cell increase from 6.7–8.6% [11]. In addition, nanomaterials with different morphologies have been used in the scattering layer of the DSSCs, including nanoplatelets, nanorods, nanofibers, etc.

However, improving the efficiency of dye-sensitized solar cells remains a major challenge. The low absorption in the visible region of TiO_2 obstructs the efficiency of DSSCs. Recently, localized surface plasmon resonance (LSPR) effect of noble metal nanoparticles such as Ag, Au and Pt has been extensively applied in photocatalysis [12] and photovoltaic devices [13]. It is reported that LSPR effect can increase the light capture rate of photoanode, thereby increasing the PCE of DSSCs [14]. The LSPR absorption is located at about 430 nm and 530 nm for spherical Ag and Au nanoparticles, respectively [15]. In addition, the LSPR effect can improve the energy level of TiO_2 to enhance the charge transfer and reduce the electron recombination. Li group synthesized Au-decorated Urchin-like TiO_2 microspheres, which makes the PCE reach to 7.21% [16]. Naphade loaded gold nanoparticles onto TiO_2 nanofibers, thus significantly improving the DSSCs performance [17].

In this work, we synthesized core-shell structure SiO_2@TiO_2 (ST) microspheres and Ag-nanoparticles (Ag NPs) decorated SiO_2@TiO_2-Ag (STA) microspheres via a simple hydrothermal method. The ST or STA microspheres were blended with P25 to manufacture composite photoanode. The improvement in performance can be attributed to the enhancement of light capture rate by strong light scattering and the enhancement of light absorption in LSPR effect due to the addition of Ag NPs. The effects and mechanisms of the STA microspheres on the performance of the DSSCs were explored.

2 Experimental

2.1 Materials and Characterization

Ethanol (EtOH, ≥ 99.7%), acetonitrile (CH_3CN, ≥ 99.7%), ammonia ($NH_3{\cdot}H_2O$, ≥ 99.7%), trisodium citrate ($C_6H_5Na_3O_7$, ≥ 99.7%), iodine (I_2, ≥ 99.7%), silver nitrate ($AgNO_3$, ≥ 99.7%), ethyl silicate (TEOS, ≥ 99.7%), (3-aminopropyl) trimethoxysilane (APTMS, ≥ 98%), 4-tert-Butylpyridine ($C_9H_{13}N$, ≥ 96%), potassium iodide (KI, ≥ 99.7%), acetone (CH_3COCH_3, ≥ 99.7%) and acetylacetone ($CH_3COCH_2COCH_3$, ≥ 99.5%) were provided by the Sinopharm Chemical Reagent Co. Ltd.. Titanium isopropoxide (TTIP, ≥ 95%) and TiO_2 NPs (P25) were purchased from Aladdin Co. Ltd.. N719 (> 95%) was obtained from Taiwan Yongguang Chemical Industry Co. Ltd.. All the water used in the experiment was deionized water. All reagents for analytical purity were used without further purification.

The crystalline structures of the samples were investigated by X-ray diffraction (XRD) carried on a DX-2700 diffractometer using the Cu Kα radiation λ = 1.5406 Å „(Fangyuan, China). The morphology and microstructure of the samples were observed with a field emission scanning electron microscope (FE-SEM, S-4800, Hitachi, Japan) and on a transmission electron microscope (TEM, JEM-2100, JEOL, Japan). The chemical elements of the samples were measured by an energy-dispersive X-ray spectroscopy (EDS, JEM-2100, JEOL, Japan). X-ray photoelectron spectroscopy (XPS) was performed on a PerkinElmer PHI 5000C ESCA instrument with Al Kα X-rays (Thermo Scientific, America). The specific surface area were

recorded on a Brunner-Emmet-Teller (BET) apparatus (ASAP2020M + C, Micromeritics, America). The optical absorption and reflection spectra were measured from the UV-vis spectrophotometer (Lambda750s, PerkinElmer, America). The current-voltage (J-V) curves of DSSCs were collected using an electrochemical Workstation (CHI 660B, China) under simulated sunlight (100 mW/cm^2). Each type of DSSCs is measured six times to reduce the error. The incident photon-to-current conversion efficiency (IPCE) was carried out by a SC S100 (Zolix, China). The electrochemical impedance spectroscopy (EIS) were measured at a bias potential of − 0.8 V with the frequency range from 0.1 Hz to 100 kHz at an ac amplitude of 10 mV using an electrochemical Workstation (CHI 660B, China) in the dark.

2.2 Preparation of SiO_2@TiO_2 (ST)

The method in the literature [18] was modified to synthesize ST. 0.12 g SiO_2 microspheres were added into the 30 mL acetonitrile and 90 mL anhydrous ethanol with ultrasonic dispersion for 30 min. The mixture was put in a 20°C water bath and added 1 mL of ammonia. After reacted for 30 min, 1 mL TTIP was slowly added to the mixture and the reaction continued for 12 h. SiO_2@TiO_2 can be obtained by centrifuging, washing and drying.

2.3 Preparation of SiO_2@TiO_2-Ag (STA)

0.35 g SiO_2@TiO_2 microspheres were dispersed in 100 mL ethanol solvent. 0.35 mL (3-aminopropyl) trimethoxysilane (APTMS) was added into solution at 80°C for 4 h to obtain the APTMS modified SiO_2@TiO_2. Subsequently, the obtained APTMS modified SiO_2@TiO_2 sample was added into 30 mL deionized water and ultrasonic for 30 min to disperse evenly. Then, 8 mg silver nitrate was added to solution stirred for 5 min at 90°C water bath and 40 mg sodium citrate was added at 90°C reacting for 30 min. Finally, Ag-nanoparticles decorated SiO_2@TiO_2 microspheres (SiO_2@TiO_2-Ag) were obtained by centrifuging and washing with deionized water.

2.4 Fabrication of DSSCs

FTO glass (2.2 mm thickness, 14 Ω/sq) was ultrasonically cleaned with acetone, ethanol and deionized water for 15 min, respectively. Briefly, the TiO_2 slurry was prepared using 0.1 g P25 powders dispersed in 0.5 mL acetylacetone. The TiO_2 slurry with three kinds of STA contents was obtained by replacing the TiO_2 slurry with the mass percentage of 1wt%, 2wt% and 3wt%. Then, the obtained slurry was coated on a FTO glass by doctor blade method with a square area of 0.25 cm^2 homogeneous films. The FTO glass was dried in an oven at 80°C and annealed at 450°C for 30 min. These photoanodes were labeled as 1%STA, 2%STA and 3%STA. The annealed photoanode was soaked in a 3.0×10^{-4} M N719 solution for 24 h in the dark. Then the anode was taken out and dried at 60°C. The counter electrode used the Pt electrode. The electrolyte solution was stirred with 0.1 M potassium iodide, 0.05 M iodine and 0.5 M 4-tert-butylpyridine in 10 mL acetonitrile for 24 h.

3 Results And Discussion

3.1 Structural and morphological characteristics

The crystal structures of the SiO_2, ST and STA were investigated by XRD. The XRD patterns were shown in Fig. 1. The diffraction pattern of SiO_2 with a broad peak at 23.5° was corresponding to that of amorphous SiO_2. The ST exhibits diffraction peaks at 25.3°, 37.9°, 48.1°, 54.0°, 55.2°, 62.8°, 70.3° and 75.2°, which were corresponding to (101), (004), (200), (105), (211), (204), (220), and (215) planes of anatase TiO_2 (JCPDS No. 21-1272). The diffraction pattern of the STA appeared peaks at 37.9°, 64.6° and 77.5° corresponding to (111), (220) and (311) planes of Ag (JCPDS No. 04-0783), respectively. The diffraction peak of Ag (111) plane and anatase TiO_2 (004) plane at 37.9° was overlapped in STA sample.

The morphology and microstructure of the as-synthesized SiO_2, ST and STA samples were investigated by SEM and TEM. It is found that SiO_2 nanospheres have good monodispersity and uniform particle size with average diameter of 350 nm (Fig. S1). It can be seen that the ST spheres with an average diameter of 400 nm are tightly coated by nano-TiO_2 shell (Fig. 2a). The STA sample shows raspberry-like rough surface, because of Ag nanoparticles were deposited on the surface of ST spheres with the reduction of silver ions by sodium citrate. The core-shell structure of STA can be discerned in Fig. 2c. Due to the effect of surface silane-amination, Ag nanoparticles were evenly dispersed on the surface of the sphere with the uniform size [19]. The HRTEM image shows that the size of Ag nanoparticle is about 10 nm. The lattice fringes were measured to be about 0.22 nm, which is corresponding to the d_{111} spacing of Ag. In addition, the elemental mapping results indicate the presence and uniform distribution of Ti, O, Si, Ag, C in STA microsphere (Fig. 3). The Si and Ti elements distribution cases further identify that the STA sphere is the core-shell structure with SiO_2 core and TiO_2 shell, while the Ag element signal is mostly scattered on the surface of STA sphere. It also confirms that core-shell structure ST modified by Ag nanoparticle dispersed uniformly on surface to form the hierarchical structure STA.

The bonding environment and the chemical state of the SAT sample was analyzed by XPS. The elements of Ti, Si, O, Ag, and C presented in the survey curve of the STA samples from the binding energies of electrons (Fig. 4a). The carbon element can be attributed to the remnant carbon form reaction. Figure 4b demonstrates that STA samples display two separated peaks for Ag 3d electron. The binding energies of 368.2 eV and 374.2 eV are corresponded to Ag $3d_{5/2}$ and Ag $3d_{3/2}$, respectively. In addition, the 6.0 eV difference of the doublet state 3d electron confirmed the formation of metallic Ag [20].

The specific surface areas of the ST and STA microspheres samples were characterized by nitrogen adsorption/desorption isotherms (Fig. S2). The BET specific surface areas were 63.25, 58.16 and 50.50 m^2/g for ST, STA and P25, respectively. The BET surface area of ST and STA microspheres was larger than that of commercial P25. The large specific surface area of ST and STA can provide more adsorption sites to increase the amount of dye adsorption, which is beneficial to the photovoltaic performance of DSSCs.

UV-vis results shown in Fig. 5 illustrate the light response of P25, ST, and STA samples. It can be seen that P25 mainly absorbs UV light below the wavelength of 400 nm because of the wide band gap of TiO_2 [21]. The absorption of P25 and ST is similar in UV region because SiO_2 has no absorption in the UV and

visible regions [22]. However, ST sample increases the absorption in the visible region obviously. The results show that SAT samples can significantly enhance the light harvest in the visible region. It is well-known that the strong absorption in the visible region is attributed to the LSPR effect of Ag NPs [23]. In addition, the LSPR effect of Ag NPs can improve the capture ability of photogenerated electrons. The reflectance of STA is distinct lower than that of P25 and ST due to light capture caused by strong LSPR of Ag NPs. The reflectance of ST is slight higher than that of P25 after the wavelength of 500 nm can be ascribed to size-dependent scattering effect [24].

3.2 Photovoltaic performances of DSSCs

Figure 6a displays the current density-voltage (J-V) curves of DSSCs based on the four different photoanodes, and the corresponding results are listed in Table 1. The different amounts of STA added into P25 has different photovoltaic properties. The current density and conversion efficiency increase with the doping amount of STA, and then decrease with the more of STA. The results show that the optimal STA to P25 ratio is 2 wt%, and the corresponding J_{sc} and PCE are 16.0 mA cm^{-2} and 7.4%, respectively. The results indicate that the PCE of the DSSCs with 2 wt% STA increased about 70% more than that of the device with pure P25 photoanode. The increase of J_{sc} and PCE may be mainly due to the light capture enhancement of LSPR effect of Ag NPs and light scattering. Moreover, the surficial Ag NPs could promote the photogenerated electron-hole separation and reduce recombination [14]. All these factors will be beneficial on photovoltaic performance of DSSCs. However, the current density and photoelectric conversion efficiency will be reduced by the excessive addition of STA. Excessive Ag may lead to electron trapped on the surface of Ag, thus reducing the current density. Meanwhile, excess Ag will increase the electron back reaction with the electrolyte when Ag is in contact with the electrolyte. The V_{oc} of the four DSSCs don't change significantly because V_{oc} is related to the energy difference between the Fermi level of TiO_2 and the redox potential in the electrolyte [25]. IPCE is an important character to evaluate the rate of light capture and quantum efficiency in DSSCs. It indicates the utilization of sunlight by DSSCs [26]. The IPCE chart of DSSCs is illustrated in Fig. 6b. Addition STA to P25 could increase the IPCE in visible region. The IPCE of DSSCs with 2 wt% STA photoanode is highest, which is consistent with the results of J-V plot. The 2 wt% STA photoanode based DSSCs exhibit the largest IPCE values in the wavelength range of 300–700 nm, which should be due to the LSPR effect of Ag NPs and the higher light scattering ability. All the IPCE results are in good agreement with the corresponding photovoltaic performance of J-V character.

Table 1 Photovoltaic properties of DSSCs based on different content of STA photoanode.

DSSCs	J_{sc}(mA/cm^2)	V_{oc}(V)	FF(%)	PCE(%)
P25	10.2	0.771	54	4.3
1%STA	12.6	0.785	56	5.5
2%STA	16.0	0.780	59	7.4
3%STA	12.1	0.777	56	5.3

The electrochemical impedance spectroscopy (EIS) was utilized to study the electron transport and recombination processes in DSSCs [27]. Figure 7a and 7b show the Nyquist and Bode plots of DSSCs. The fitting data of equivalent circuit are presented in Table 2. It can be seen there are two semicircles of P25 photoanode in Fig. 7a. The larger semicircle represents the interface transfer impedance R2 and stands for the photoanode/dye/electrolyte interface in DSSCs. The small semicircle stands for the Pt electrode-electrolyte interface R3. The intercept on the real axis represents the series resistance R1 in the equivalent circuit. Since the Pt electrode and external circuit are used in same testing condition, different DSSCs should show similar R3 and R1. The R2 is inversely related to the J_{sc} of DSSCs. R2 of 2 wt% STA photoanodes decreased significantly which indicated the modification of Ag will improve the electron transport rate in DSSCs and lessen the recombination of electrons and holes in DSSCs. Furthermore, when the amount of STA doping continues to increase, excessive Ag may become a recombination center that is not conducive to the charge transfer process, leading to an increase in R2. The FF value reflects the parameter related to the intrinsic resistance of DSSCs, so the decrease of R2 can explain the increase of the FF value of DSSCs [28].

Table 2 Electron dynamic parameters estimated from the Nyquist and Bode phase plots

DSSCs	R2(Ω)	f_{max}(Hz)	τ(ms)
P25	61.58	21.54	7.39
1%STA	42.38	17.78	8.95
2%STA	35.71	10.00	15.91
3%STA	46.57	14.68	10.84

The electron lifetime (τ) in DSSCs can be evaluated from the Bode phase plots of EIS on the basis of the equation $\tau = 1/(2\pi f_{max})$ [29], where f_{max} is the maximum peak frequency. As shown in Fig. 7b, the peak of doped STA photoanode moved to the low frequency direction compared to pure P25, indicating that addition of STA could prolong the electron lifetime. The τ of 2wt% STA of DSSCs (15.91 ms) are greater than that pure P25 of DSSCs (7.39 ms). These further confirmed that the addition of an appropriate amount of STA will benefit the electron transfer inside the photoanode, reduce charge recombination and promote the conversion efficiency of DSSCs.

The sandwiched DSSCs cell structure and reaction mechanism are presented in Fig. 8. The dye (N719) molecule becomes excited state after absorbing photon energy under light irradiation. It produces an electronic transition from the highest occupied molecular orbital (HOMO) to the lowest unoccupied molecular orbital (LUMO). The photo-excited electrons jump from dye (N719) into the CB of TiO_2 and then inject to the adjacent Ag NPs. At the same time, P25 nanoparticles also absorb short wavelength photons energy to generate electrons and holes in conduction band and valence band respectively. Due to the continuous band structure of Ag NPs, the electron mobility from TiO_2 to Ag NPs will remain at the continuous energy level near the Fermi level. Meanwhile, the injected electrons in the CB of TiO_2 transferred to the conductive substrate (FTO). Finally, the electrons move from the external circuit to the Pt electrode. The photogenerated electrons collected by the Ag NPs will promote the charge separation

process. Therefore, Ag NPs can decrease the electron recombination reaction from the CB of TiO_2 to the dye and a back reaction with the electrolyte. SiO_2/TiO_2 core-shell sphere is used as scattering medium center of Ag surface plasma and incident light. Altogether, the proposed STA will improve the efficiency of electron collection and provide beneficial influence on the property of DSSCs.

4 Conclusion

In short, we successfully synthesized $SiO_2@TiO_2$-Ag core-shell spheres modified by Ag nanoparticles on the surface. The as-prepared STA spheres are used as efficient multifunctional scatter introduced into P25 powder to construct composite photoanode. The DSSCs of 2 wt% STA in photoanode possesses the highest current density of 16.0 mA cm^{-2} and conversion efficiency of 7.4%, which is obviously high than that of pure P25 DSSCs. The LSPR effect of surface Ag nanoparticles broadens the visible light absorption of DSSCs and promotes the photogenerated electron-hole separation.

Declarations

Acknowledgements

This research is financially supported by the National Natural Science Foundation of China (No. 21404001, 51472001), the Anhui Province University Natural Science Research Project (No. KJ2020A0014).

Conflict of Interest: The authors declare that they have no conflict of interest.

References

[1] B. Oregan, M. Gratzel, A low-cost, high-efficiency solar cell based on dye-sensitized colloidal TiO_2 films. Nat. **353**, 737-740 (1991)

[2] A. Hagfeldt, G. Boschloo, L. Sun, L. Kloo, H. Pettersson, Dye-sensitized solar cells. Chem. Rev. **110**, 6595-6663 (2010)

[3] M. Ye, X. Wen, M. Wang, J. Iocozzia, N. Zhang, C. Lin, Z. Lin, Recent advances in dye-sensitized solar cells: from photoanodes, sensitizers and electrolytes to counter electrodes. Mater. Today **18**, 155-162 (2015)

[4] D. Zhao, L. Niu, L. Wang, Plasmon enhanced heterogeneous electron transfer with continuous band energy model. Chem. Phys. **493**, 194-199 (2017)

[5] M. Yu, Y.B. Meng, J.D. Zhang, J.H. Liu, S.M. Li, Super helical Au/TiO_2 nanocomposites based on plasmid DNA for efficiency dye-sensitized solar cells. J. Mater. Sci.-Mater. Electron. **28**(5), 4138-4145 (2016)

[6] M.S. Wu, Z.Z. Ceng, C.Y. Chen, Surface modification of porous TiO_2 electrode through pulse oxidative hydrolysis of $TiCl_3$ as an efficient light harvesting photoanode for dye-sensitized solar cells. Electrochim. Acta **191,** 256-262 (2016)

[7] A. Kunzmann, M. Stanzel, W. Peukert, R.D. Costa, D.M. Guldi, Binary indium-zinc oxide photoanodes for efficient dye-sensitized solar cells. Adv. Energy Mater. **6**, 1501075 (2016)

[8] R.K. Chava, W.M. Lee, S.Y. Oh, K.U. Jeong, Y.T. Yu, Improvement in light harvesting and device performance of dye sensitized solar cells using electrophoretic deposited hollow TiO_2 NPs scattering layer. Sol. Energy Mater. Sol. Cells **161**, 255-262 (2017)

[9] J. Yu, Q. Li, Z. Shu, Dye-sensitized solar cells based on double-layered TiO_2 composite films and enhanced photovoltaic performance. Electrochim. Acta **56**, 6293-6298 (2011)

[10] S. Son, S.H. wang, C. Kim, J. Yun, J. Jang, Designed synthesis of SiO_2/TiO_2 core/shell structure as light scattering material for highly efficient dye-sensitized solar cells. Acs Appl. Mater. Interfaces **5**, 4815-4820 (2013)

[11] B. Tan, Y. Wu, Dye-sensitized solar cells based on anatase TiO_2 nanoparticle/nanowire composites. J. Phys. Chem. B **110**, 15932-15938 (2006)

[12] Z. Liu, W. Hou, P. Pavaskar, M. Aykol, S.B. Cronin, Plasmon resonant enhancement of photocatalytic water splitting under visible illumination. Nano Lett. **11**, 1111-1116 (2011)

[13] A.P. Kulkarni, K.M. Noone, K. Munechika, S.R. Guyer, D.S. Ginger, Plasmon-enhanced charge carrier generation in organic photovoltaic films using silver nanoprisms. Nano Lett. **10**, 1501-1505 (2010)

[14] C. Liu, T. Li, Y. Zhang, T. Kong, C. Li, Silver nanoparticle modified TiO_2 nanotubes with enhanced the efficiency of dye-sensitized solar cells. Microporous Mesoporous Mater. **287**, 228-233 (2019)

[15] Y. Li, Y. Zhou, Y. Wang, R. Zhou, Q. Ling, H. Niu, W. Zhang, C. Wang, J. Qiu, Z. Guo, Au nanoparticle-decorated urchin-like TiO_2 hierarchical microspheres for high performance dye-sensitized solar cells. Electrochim. Acta **293**, 230-239 (2019)

[16] Y. Li, H. Wang, Q. Feng, G. Zhou, Z.S. Wang, Gold nanoparticles inlaid TiO_2 photoanodes: a superior candidate for high-efficiency dye-sensitized solar cells. Energy Environ. Sci. **6**, 2156-2165 (2013)

[17] R.A. Naphade, M. Tathavadekar, J.P. Jog, S.A. Agarkar, S.B. Ogale, Plasmonic light harvesting of dye sensitized solar cells by Au-nanoparticle loaded TiO_2 nanofibers. J. Mater. Chem. **2**, 975-984 (2014)

[18] M. Li, N. Yuan, Y. Tang, L. Pei, Y. Zhu, J. Liu, L. Bai, M. Li, Performance optimization of dye-sensitized solar cells by gradient-ascent architecture of SiO_2@Au@TiO_2 microspheres embedded with Au nanoparticles. J. Mater. Sci. Technol. **35**, 604-609 (2019)

[19] J. Choma, A. Dziura, D. Jamio A, P. Nyga, M. Jaroniec, Preparation and properties of silica–gold core–shell particles. Colloid Surf. A-Physicochem. Eng. Asp. **373**, 167-171 (2011)

[20] Z. Jiang, W. Wei, D. Mao, C. Chen, Y. Shi, X. Lv, J. Xie, Silver-loaded nitrogen-doped yolk-shell mesoporous TiO_2 hollow microspheres with enhanced visible light photocatalytic activity. Nanoscale **7**, 784-797 (2014)

[21] Y. Zhang, Z.Y. Zhao, J.R. Chen, L. Cheng, J. Chang, W.C. Sheng, C.Y. Hu, S.S. Cao, C-doped hollow TiO_2 spheres: in situ synthesis, controlled shell thickness, and superior visible-light photocatalytic activity. Appl. Catal. B-Environ. **166**, 715-722 (2015)

[22] D. Hu, Y. Huang, H. Liu, H. Wang, S. Wang, M. Shen, M. Zhu, X. Shi, The assembly of dendrimer-stabilized gold nanoparticles onto electrospun polymer nanofibers for catalytic applications. J. Mater. Chem. **2**, 2323-2332 (2014)

[23] K.P.O. Mahesh, D. Kuo, B. Huang, Facile synthesis of heterostructured Ag-deposited SiO_2@TiO_2 composite spheres with enhanced catalytic activity towards the photodegradation of AB 1 dye. J. Mol. Catal. A-chem. **396**, 290-296 (2015)

[24] H. Koo, J. Park, B. Yoo, K. Yoo, K. Kim, N. Park, Size-dependent scattering efficiency in dye-sensitized solar cell. Inorg. Chim. Acta **361**, 677-683 (2008)

[25] Y. Li, J. Wang, X. Liu, C. Shen, K. Xie, B. Wei, Au/TiO_2 hollow spheres with synergistic effect of plasmonic enhancement and light scattering for improved dye-sensitized solar cells. ACS Appl. Mater. Interfaces **9**, 31691-31698 (2017)

[26] H. Chen, C.Y. Hong, C. Kung, C. Mou, K.C.W. Wu, K. Ho, A gold surface plasmon enhanced mesoporous titanium dioxide photoelectrode for the plastic-based flexible dye-sensitized solar cells. J. Power Sources **288**, 221-228 (2015)

[27] Y. Zhao, J. Zhai, T. Wei, L. Jiang, D. Zhu, Enhanced photoelectrical performance of TiO_2 electrodes integrated with microtube-network structures. J. Mater. Chem. **17**, 5084-5089 (2007)

[28] Q. Wang, J. Moser, M. Gratzel, Electrochemical impedance spectroscopic analysis of dye-sensitized solar cells. J. Phys. Chem. B **109**, 14945-14953 (2005)

[29] M. Adachi, M. Sakamoto, J. Jiu, Y. Ogata, S. Isoda, Determination of parameters of electron transport in dye-sensitized solar cells using electrochemical impedance spectroscopy. J. Phys. Chem. B **110**, 13872-13880 (2006)

Figures

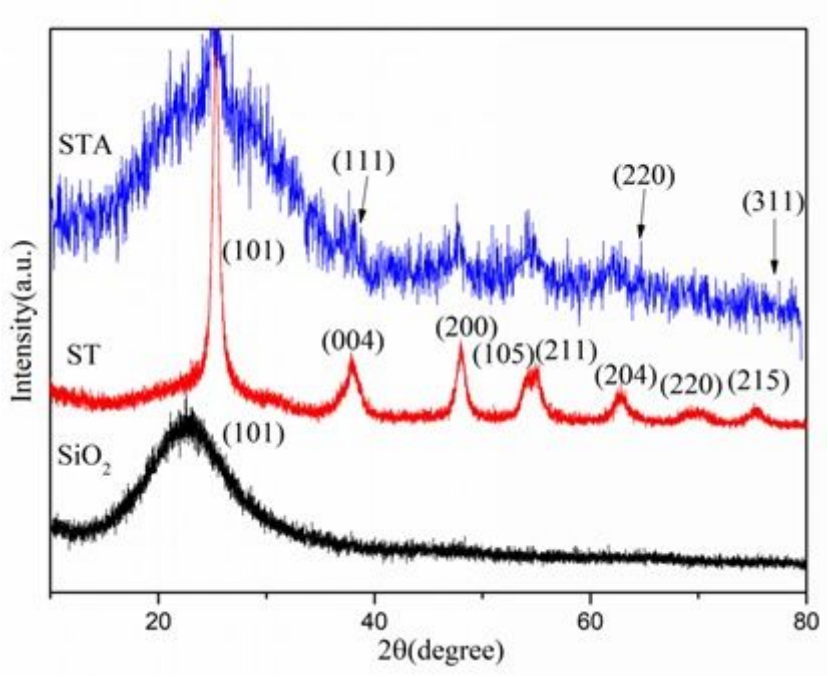

Figure 1

X-ray diffraction pattern of as-synthesized SiO2, ST and STA.

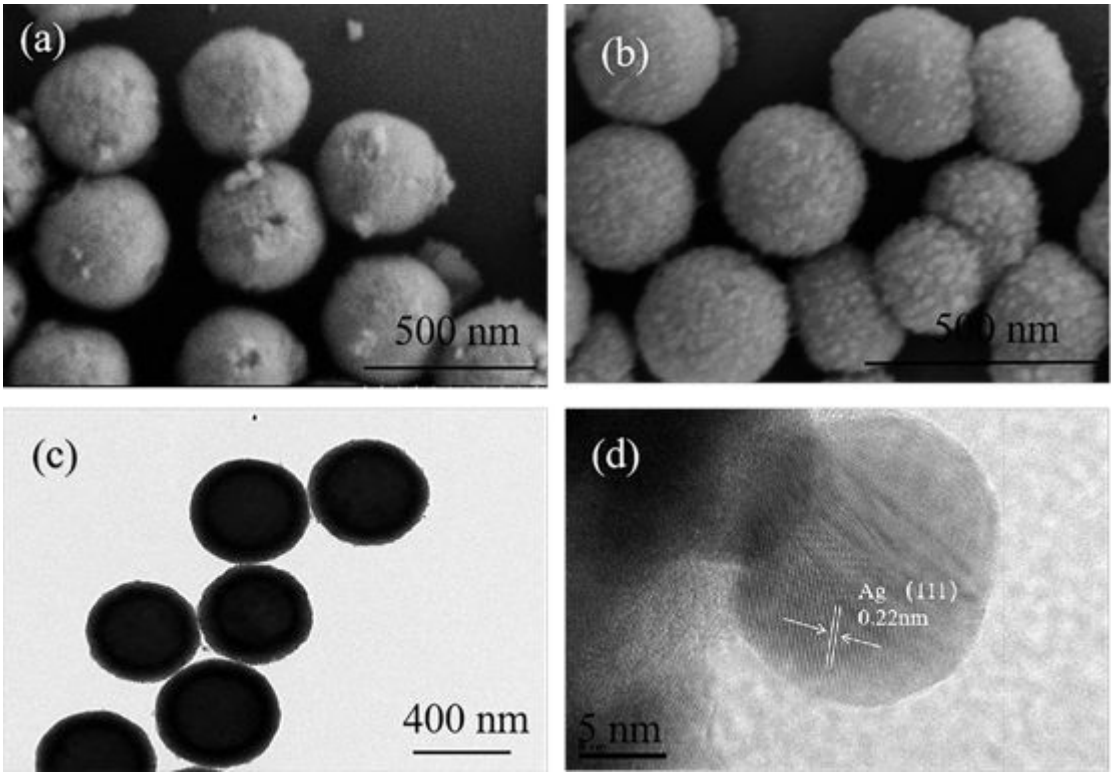

Figure 2

SEM images of ST (a), STA (b), TEM and HRTEM image of STA (c, d).

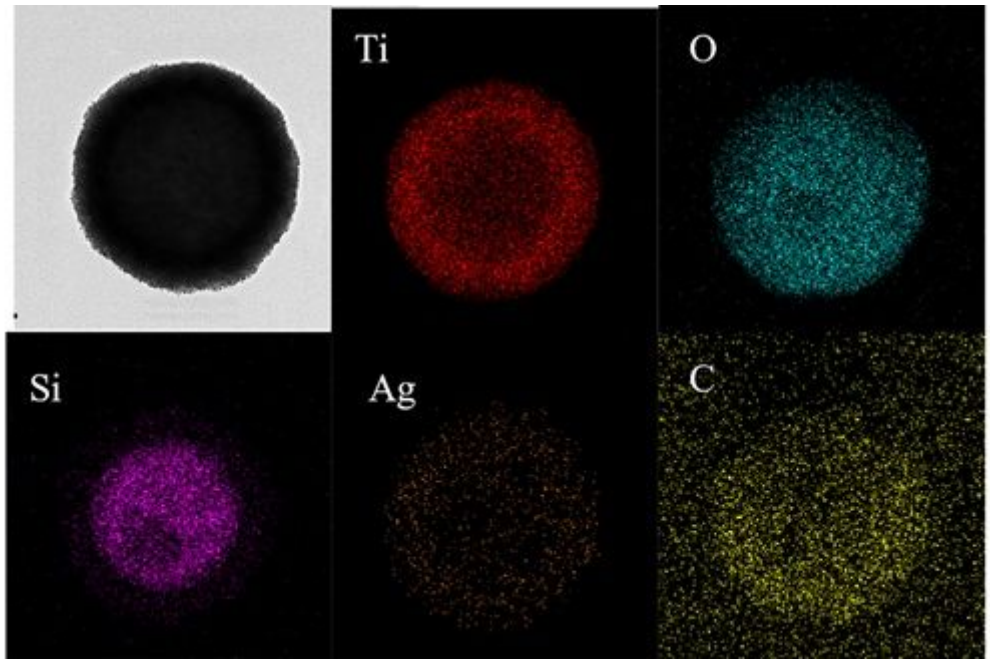

Figure 3

Elemental mapping of STA microspheres.

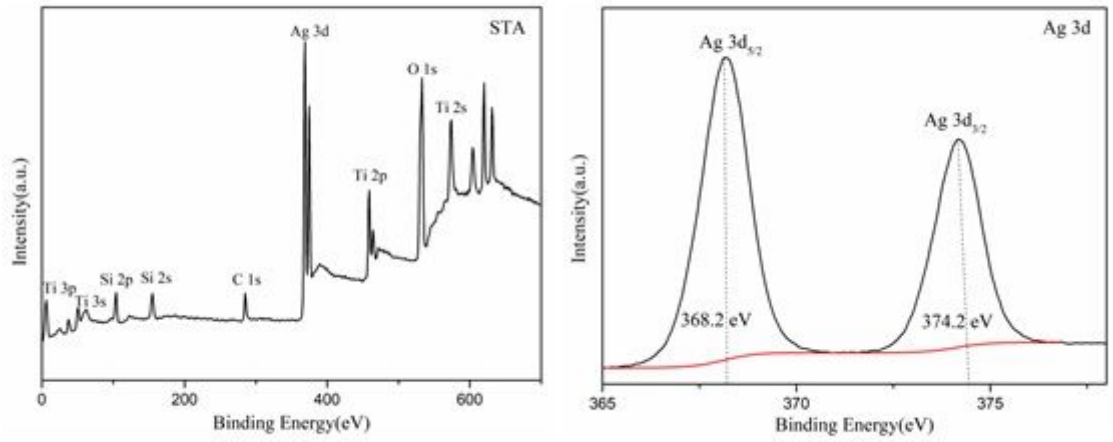

Figure 4

The XPS spectra of of STA (a) survey and (b) Ag 3d.

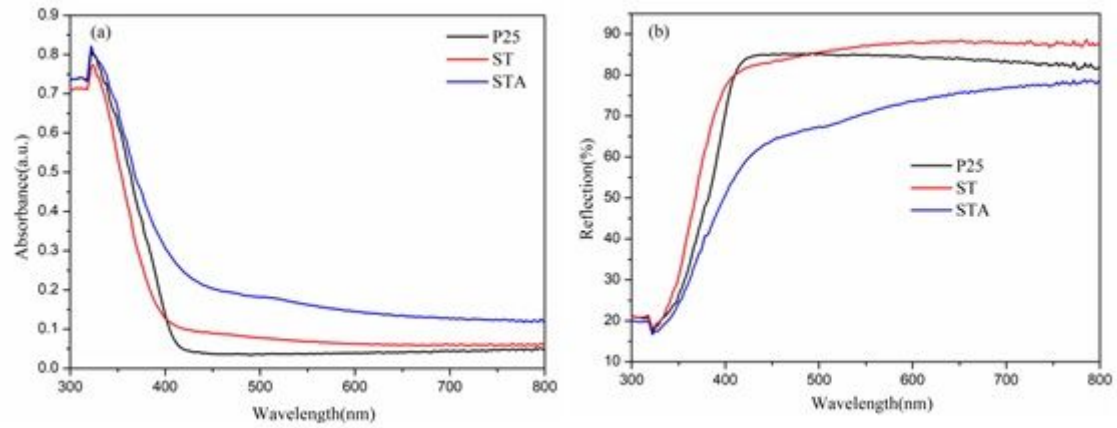

Figure 5

UV-vis absorption spectra (a) and diffused reflectance spectra (b) of P25, ST and STA.

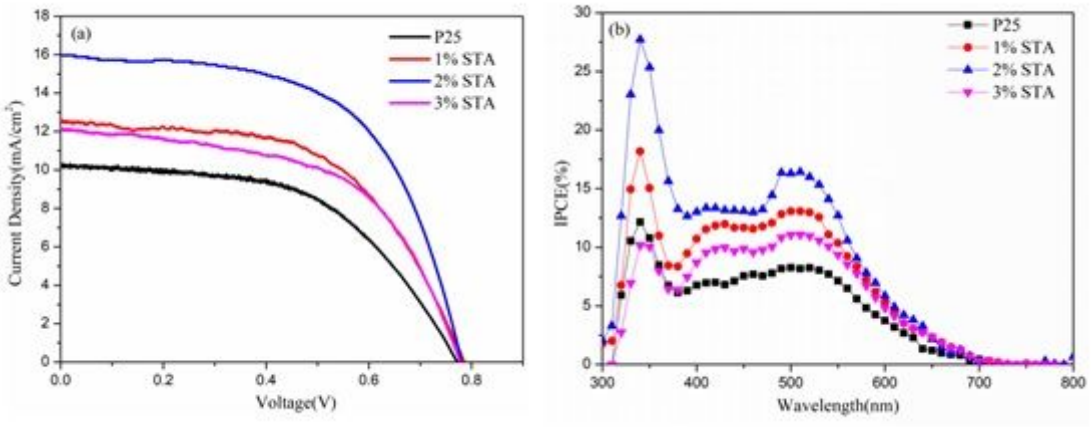

Figure 6

J-V curves (a) and IPCE spectra (b) of DSSCs fabricated with different photoanode.

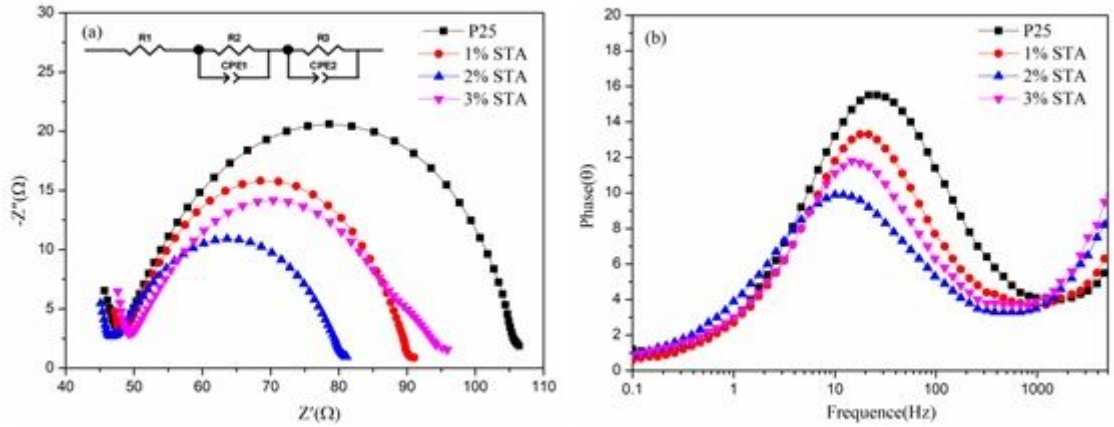

Figure 7

Nyquist plots (a) and Bode phase plots (b) of EIS spectra of the DSSCs.

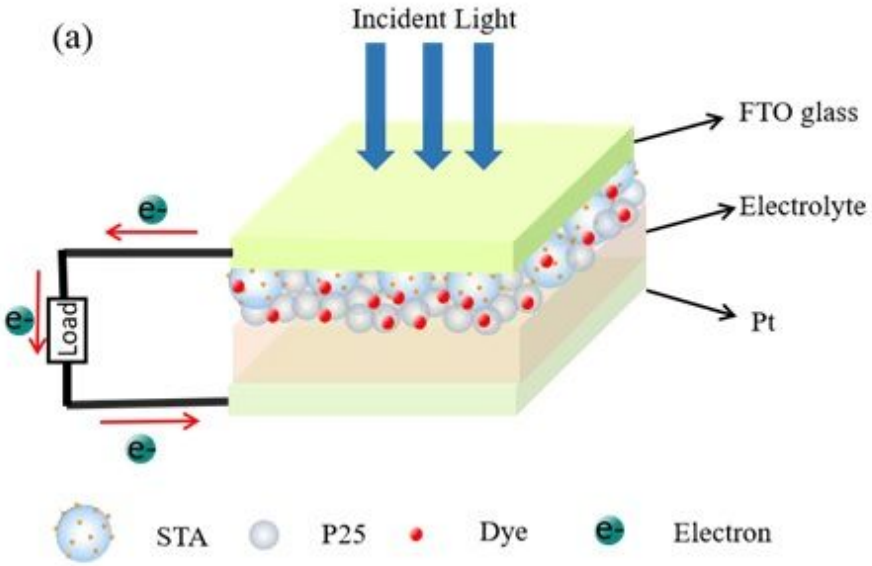

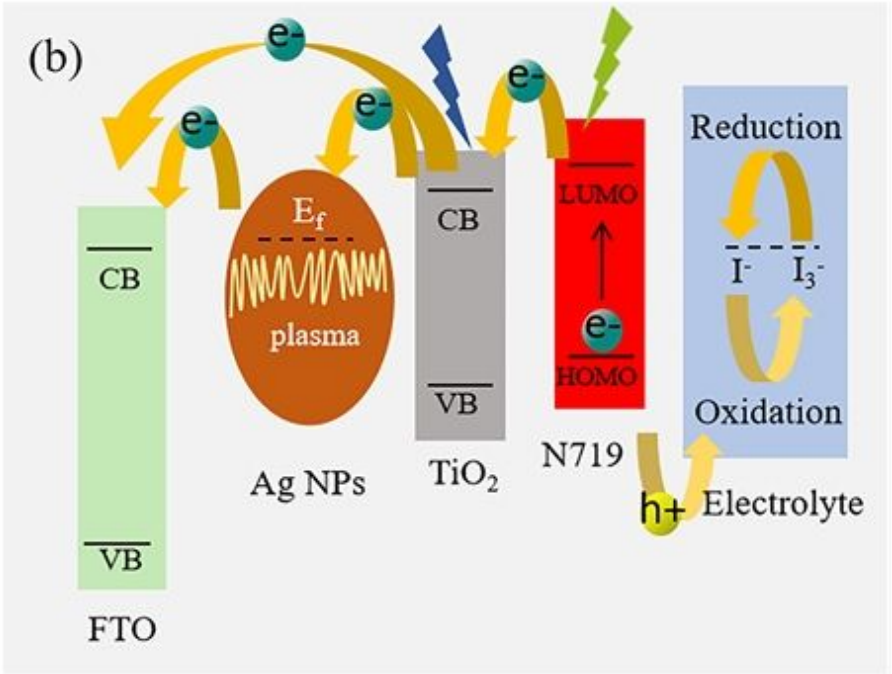

Figure 8

Sandwiched DSSCs structure (a) and proposed mechanism diagram (b)